ACADEMIC PRESS

Available online at www.sciencedirect.com
SCIENCE DIRECT®

Journal of Colloid and Interface Science 262 (2003) 16–24

JOURNAL OF Colloid and Interface Science

www.elsevier.com/locate/jcis

Priority communication

Spontaneous absorption of viscous and viscoelastic fluids by capillaries and porous substrates

Alexander V. Bazilevsky,[a] Konstantin G. Kornev,[b] Aleksey N. Rozhkov,[a] and Alexander V. Neimark [b,*]

[a] *Institute for Problems in Mechanics RAS, 101(1) Prospect Vernadskogo, Moscow 119526, Russia*
[b] *Center for Modeling and Characterization of Nanoporous Materials, TRI/Princeton, P.O. Box 625, Princeton, NJ 08542, USA*

Received 4 October 2001; accepted 22 October 2002

Abstract

We have developed a new technique to monitor spontaneous absorption of fluids by porous substrates. The method is based on an optical electronic measuring system providing millisecond resolution. The method capabilities are demonstrated with the example of the absorption of millimeter-size droplets of water and aqueous solutions of polyethylene oxide and polyacrylamide by capillaries. It is shown that polymer additives even in a small amount reduce significantly the rate of absorption. We have introduced a generalized Lucas–Washburn equation to account for the fluid elasticity. This equation is shown to explain the observed kinetics quantitatively without invoking adjustable parameters. We have derived a modified Bosanquet equation for the initial velocity of penetration, which accounts for the fluid elasticity. This simple formula gives a reasonable estimate of the rate of absorption of small droplets. We report visualization experiments on absorption of water and polymer solutions by sugar cubes as an example of porous substrates. Although the kinetics of droplet adsorption by porous substrates is similar to the kinetics of droplet adsorption by capillaries, the interpretation of experimental data is more complex and requires a plausible hydrodynamic model for lateral spreading in pores.

1. Introduction

Spontaneous penetration of viscous and viscoelastic fluids into pores is observed in various natural and physiological processes and has numerous applications in medicine and biomedical engineering, cosmetics and personal care, oil recovery and agriculture, catalysis and separations, paper and fiber industries, etc. [1–5]. This process may be very fast. As shown below, a millimeter-size droplet of water is completely absorbed by a sugar cube within ~ 0.01 s. Fast absorption was studied by high-speed photography of propagating menisci in transparent capillaries [6–8]. We have developed a new technique applicable to various substrates. Instead of monitoring the position of the liquid front in pores, we follow with millisecond resolution the change in volume/radius of the droplet residing atop the substrate. The method is based on an optical electronic measuring system that has significant advantages over commercially available high-speed photography.[1]

In the proposed method,[2] a syringe–substrate assembly is placed between a light source and an optical sensor as shown in Fig. 1a. A droplet is emitted and as soon as it touches the substrate the fluid penetrates into the pores. Schematic sketches of characteristic stages of droplet absorption by a capillary are given in Fig. 1b. The luminous flux propagating through the gap between the needle of the syringe and the substrate is measured during the process of absorption. An analysis of the dynamics of droplet absorption is reduced to an interpretation of the optical signal. The intensity of the luminous flux is controlled by the cross-sectional area of the droplet residing in the gap at a given instant in time. In the instrument embodiment, the signal displayed on the screen is a transformation of the real optical signal. We

* Corresponding author.
E-mail address: aneimark@triprinceton.org (A.V. Neimark).

[1] After our article was submitted, there appeared a very interesting article [9] where high-speed photography was employed to analyze droplet absorption by porous substrates.

[2] Patent pending.

0021-9797/03/$ – see front matter
doi:10.1016/S0021-9797(02)00045-0

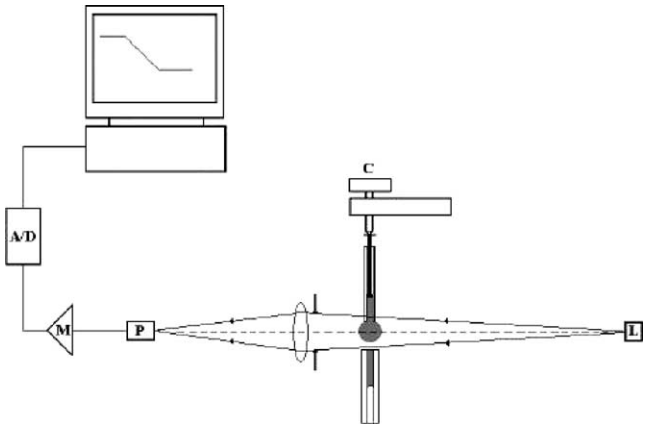

(a)

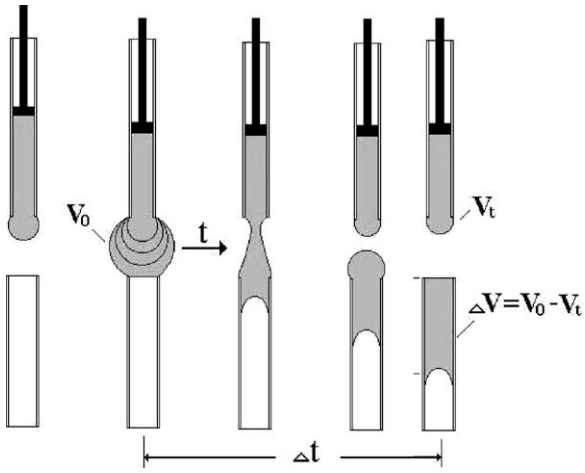

(b)

Fig. 1. (a) Experimental setup for studying the droplet absorption. L, light source; P, photodiode; M, multiplier; A/D, analog/digital converter (A/D); C, dozing screw. (b) Sequence of events featuring the droplet absorption by capillary.

read the luminous flux blocked by the droplet. That is, the signal decreases as the droplet penetrates into the substrate. In the simplest version of the method, we measure the time interval Δt between droplet formation and its disappearance due to complete absorption (Fig. 1b). Since the initial droplet suspended at the needle is almost spherical, the optical signal is easily calibrated into the droplet volume V_0 with high accuracy. The amount of absorbed liquid ΔV is calculated as the difference between the initial volume V_0 and the volume V_t of the residual droplet attached to the needle. Thus, the rate of absorption is quantified by the average volumetric flow rate $Q = \Delta V/\Delta t$. Absorption by a capillary can be quantified by the average fluid velocity U given by the formula $U = Q/\pi R^2$ (R—radius of the capillary).

The method can be used for characterization of a wide range of different porous substrates. Among them are capillaries, solid and soft membranes, rough surfaces, yarns, etc. The technique can be also applied to quantitative analyses of the wettability, permeability, and sorption capacity of structured substrates, including chips for microfluidic devices, nano and micro electromechanical systems, chips for protein recognition, and the like [10].

In this paper we first describe the experimental set-up and then discuss the difference between the absorption kinetics of viscous and viscoelastic fluids.

2. Instrumentation

As shown in Fig. 1a, the optical measuring system consists of a light source (L) and a photodiode (P) with a multiplier (M). The system is connected to a computer through an analog/digital converter (A/D). As the droplet is emitted from the syringe by a dozing screw (C), the signal is processed to determine the droplet volume V_0 and the time of droplet absorption Δt.

We illustrate the method of determination of parameters V_0 and Δt by using a typical form of the signal in Fig. 2. The left ascending branches correspond to the bulging droplets shown schematically in the second frame of Fig. 1b. The descending fragments in Fig. 2 correspond to the process of absorption, the characteristic stages of which are sketched in frames [3–5] of Fig. 1b. The right ascending branches manifest the appearance of the next droplet at the needle edge. The time interval between the maximum and the minimum of the signal curve in Fig. 2 corresponds to the time of droplet absorption Δt. Assuming that the droplet has a spherical shape when the signal is maximal, we obtain the initial droplet volume V_0. The volume V_t (Fig. 1b) associated with the minimum in Fig. 2 is calculated by considering the residual droplet as a spherical cup. The assumption of the droplet sphericity is justified by the visualization of the process (see Section 3).

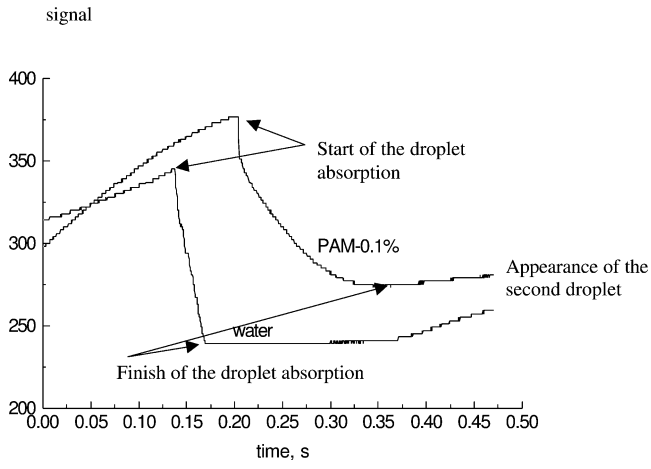

Fig. 2. Example of the records of optical signals (arbitrary units) during absorption of a water droplet and of a droplet of polyacrylamide solution by a capillary.

3. Material characterization

We used distilled water, aqueous solutions of polyethyleneoxide (PEO) of molecular mass of 4×10^6, and polyacrylamide (PAM) of molecular mass 11×10^6. The stainless-steel capillaries of 0.46- and 0.65-mm diameter, glass capillaries of 0.65-mm inner diameter, and sugar cubes were used as model absorbents. A detailed analysis of the absorption phenomenon was performed on glass capillaries 0.65 mm diameter. To provide the data on reproducibility, the capillary was carefully cleaned with water, then with a 2% aqueous solution of NaOH, and then with water again. Finally, the capillary was dried with air at room temperature.

The surface tension of liquids was measured by the drop weight method of Tate with the correction factor given in [11]. The measurements were done with the same instrument. The data are summarized in Table 1.

The stages of the absorption process were demonstrated in a series of visualization experiments. Figures 3–5 show some video frames taken during droplet absorption. The images confirm the assumption that the droplet remains spherical until it touches the substrate. As soon as contact is established and absorption begins, a bridge linking the droplet and needle is formed. Although the time intervals are very small, they are sufficient for stress relaxation. Thus, the contact line is kept pinned to the needle brim, and, in accord with a traditional scheme of droplet formation, the droplet detachment is associated with breakdown of the bridge [2]. While the process of bridge rupture is almost unaffected by the substrate properties, we observe a striking difference between absorption of water and absorption of polymer solutions. The first four frames in Figs. 4 and 5 are almost identical and the time intervals between them are comparable. That is, the polymer additives do not affect significantly the hydrodynamics of bridge formation. However, they do affect the droplet snap off at the late stages when the bridge neck transforms into a thin filament. Almost cylindrical filaments were detected recently for water droplets as well, but they disappear swiftly [12]. The stability of filaments formed by PEO solutions reflects the effect inherent in macromolecular solutions: during the bridge thinning the coils are stretched, thus forming a bundle of "pins" stabilizing the filament [12–14]. The filament lifetime is an order of magnitude longer than the time of bridge formation. Thus, fluid rheology influences the process of droplet detachment significantly by increasing the lifetime of the bridge. However, the presence of the filament linking the absorbing droplet and the needle does not affect the measured rate of absorption. Indeed, the cross-sectional area of the filament is much smaller than the cross-sectional area of the droplet and, consequently, the contribution of the filament to the reading signal during droplet absorption

Table 1
Experimental values of parameters measured at room temperature 20–22 °C and used in computations[a]

	PAM	PEO	PAM	PEO	PAM	PAM	PAM	PEO	Water
Concentration (ppm)	10	10	100	100	200	500	1000	1000	0
Surface tension (mN/m)	71.7	69.9	71.7	62.5	70.9	70.2	69.4	61.8	71.7
Relaxation time (10^{-2} s)	0.33[b]	0.16[b]	2.7	0.8	5	11	20	5	0
Viscosity (mPa s)	4	1	4	1	4	4	16	4	1
Average flow rate (mm^3/s)	104	220	51	112	38	24	7	69	220
$\pi R^2 \cdot U_{VE}$ (mm^3/s)	127	195	53	138	39	27	10	37	220

[a] U_{VE} is defined by Eq. (3).
[b] The values obtained by fitting the curve of relaxation time versus concentration.

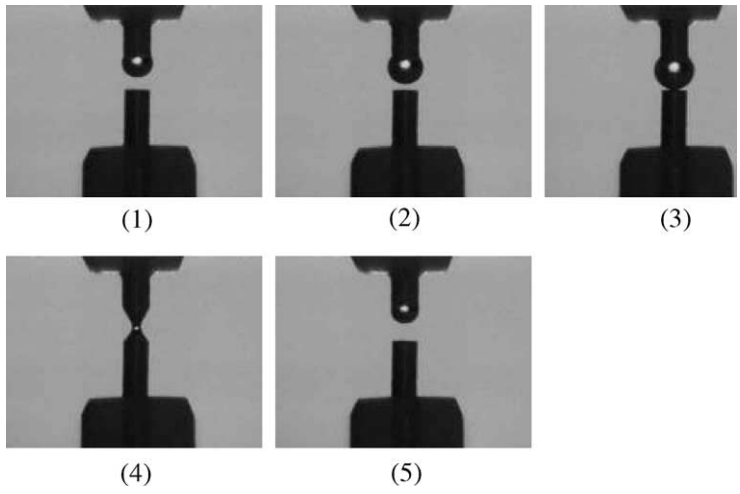

Fig. 3. Absorption of a water droplet by a stainless-steel capillary. The time intervals between the first, second, and third images are about 1 s. The process takes about 10 ms between the third and fifth images.

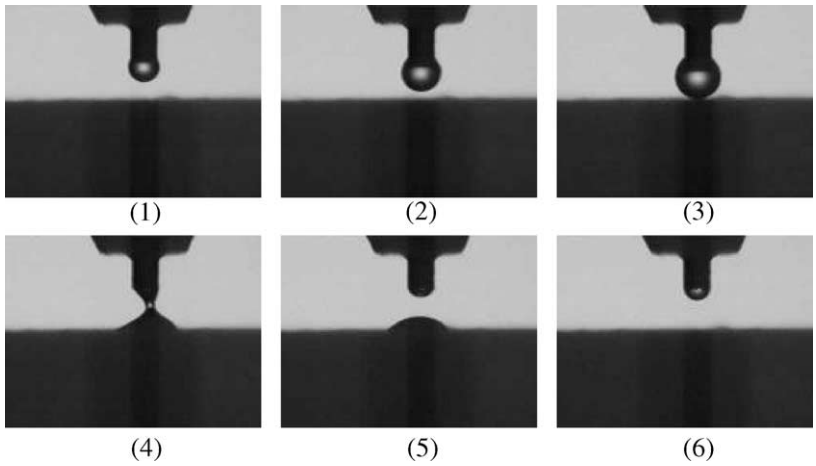

Fig. 4. Absorption of a water droplet by a sugar cube. The time intervals between the first, second, and third images are about 1 s; between the last four, 2–3 ms.

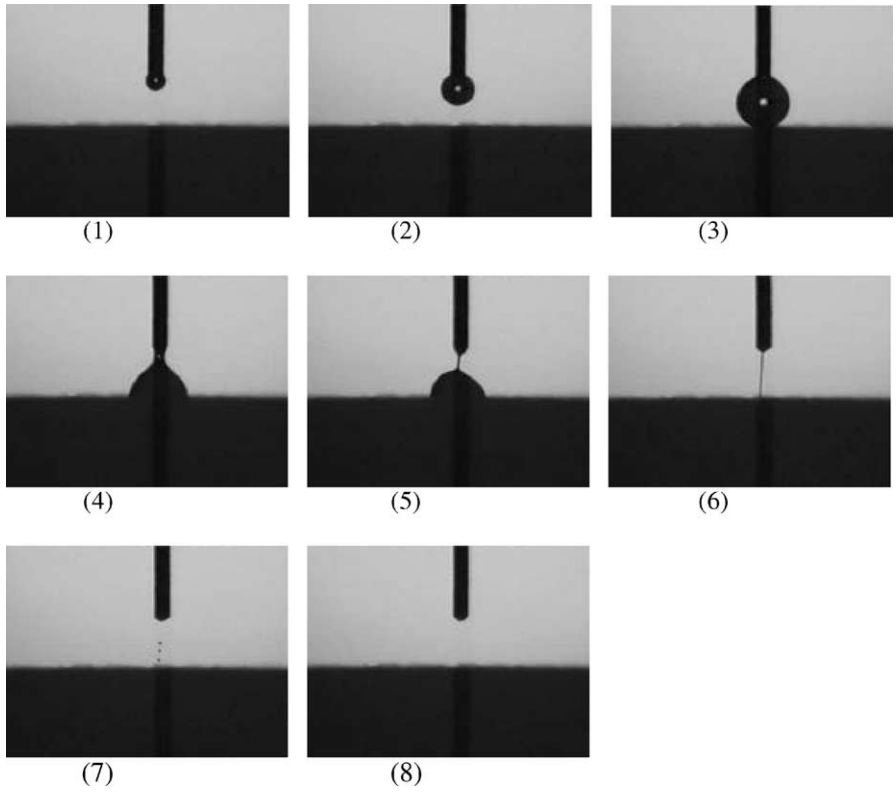

Fig. 5. Absorption of a droplet of 100 ppm PEO solution ($\lambda = 0.02$ s) by a sugar cube. The time intervals are: between the first, second, and third images, 2–3 s; between the third, fourth, and fifth images, 2–3 ms; between the fifth and sixth images, 14–16 ms; between the sixth and eighth images, 0.5 s.

is negligible. For large droplets ($\gtrapprox 2$ mm^3) formed from concentrated polymer solutions ($\gtrapprox 500$ ppm) the filament radii are greater than those depicted in Fig. 5. However, the optical signal has two well-distinguished regions: the first is associated with the droplet disappearance and the second is attributed to the dynamics of filament thinning. Thus, the time of droplet absorption can be found with high accuracy as a point where the steeply decreasing region transforms into a shallow one. Though the presence of the filament does not affect the absorption rate directly, it is a sign that fluid elasticity may play an important role in the process. Moreover, the phenomenon of filament thinning seems to be a promising tool for determination of the relaxation time simultaneously with measurement of the droplet absorption rate [15]. We are currently modifying the instrument to include this option.

For quantitative characterization for polymer solutions, a coaxial cylinder viscosimeter was used to measure the shear viscosity of the liquids. As we see from the rheological measurements (Fig. 6), in the range of large shear rates the

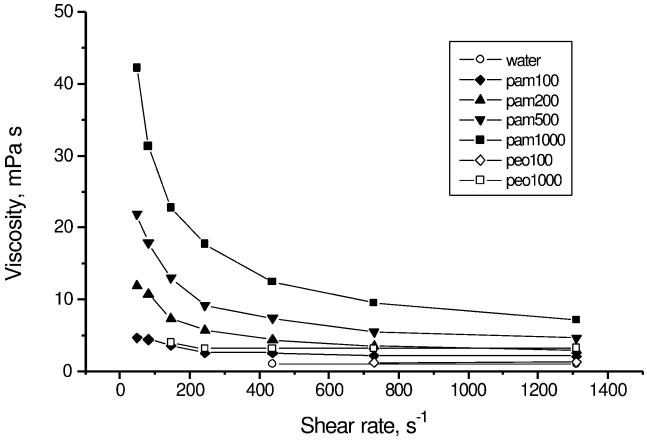

Fig. 6. Viscosity of different solutions as a function of shear rate.

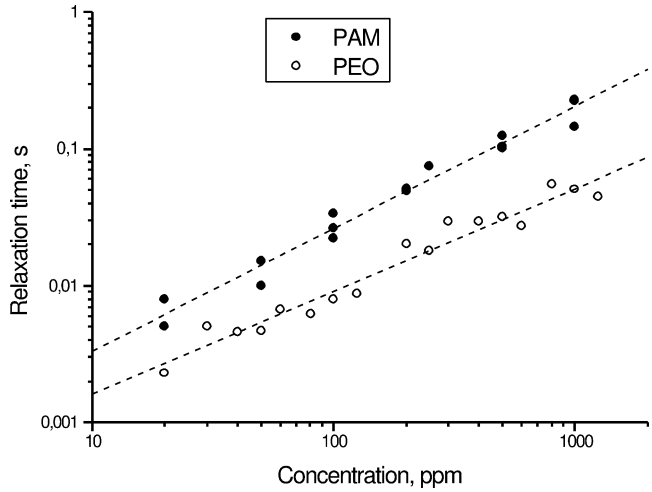

Fig. 7. Relaxation time as a function of PAM and PEO concentration. Fitting lines: for PAM $\lambda = 10^A C^B$, $A = -3.373 \pm 0.089$, $B = 0.894 \pm 0.039$; for PEO $\lambda = 10^A C^B$, $A = -3.543 \pm 0.087$, $B = 0.750 \pm 0.038$.

shear viscosity η may be approximated by a constant. The high shear rates are typical of the process of absorption. Indeed, the shear rate can be evaluated as $\Gamma = U/R$, where U is the velocity of fluid penetration, and R is the capillary radius. Taking $U \sim 15$ cm/s and $R = 0.3$ mm we estimate the shear rate as $\sim 500\ \mathrm{s}^{-1}$. At such large shear rates, $\Gamma \gtrsim 100\ \mathrm{s}^{-1}$, the shear viscosity of PEO solutions is practically the same as that of water, 1 mPa s. At the same time, PAM solutions show non-Newtonian behavior, especially in the range of shear rates between 100 and $500\ \mathrm{s}^{-1}$ (Fig. 6). As the shear rate increases further, the viscosity of PAM solutions tends to a certain limiting value. For 200 ppm solution, this value is approximately four times larger than the viscosity of water, while the viscosity of 500–1000 ppm solutions is about 10 times greater than that of water.

The visualization experiments point out that the fluid elasticity must be taken into account for polymer solutions. To quantify fluid elasticity we invoke the Maxwell model. Being quite simple, this model is suitable for fluids, which, from one side, have a constant shear viscosity, and, from the other side, show an elastic response [13–16]. While keeping the viscosity Newtonian, the Maxwell model accounts for the elastic properties of the fluid through a special parameter called the relaxation time λ. The latter is estimated as the time that is needed for a polymer coil to assume its spheroidal shape after deformation. Monitoring the kinetics of filament thinning under stretching, and assuming a stagnation point flow in the filament, the relaxation time can be extracted from images akin to those in Fig. 5 [12,15,17,18]. The extensional rheotester [14,15,17,18] was used to measure the relaxation time by analyzing the images of the filament during its thinning. The data are summarized in Fig. 7.

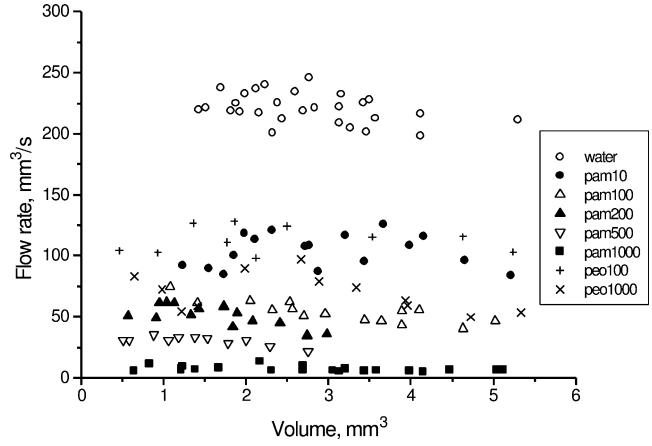

Fig. 8. Experimental data on absorption of water and polymer solutions by glass capillaries.

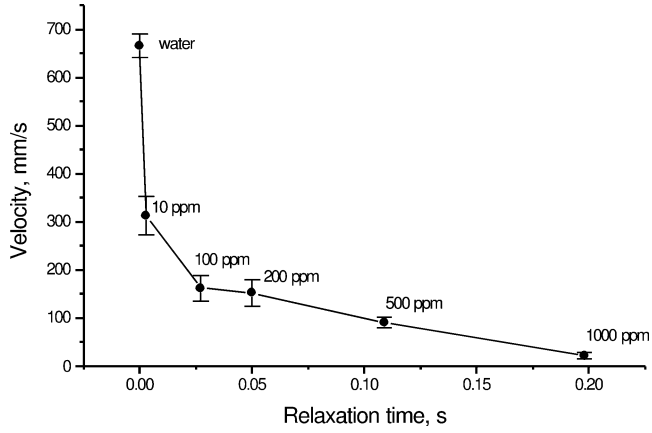

Fig. 9. Rate of absorption of droplets of PAM solutions as a function of the relaxation time. The mass concentration is specified for each point. The error bar represents the deviations of the absorption rates for the droplets of different size.

4. Rheological effects in the dynamics of droplet absorption

The dynamics of droplet absorption by capillaries is quantitatively characterized by Figs. 2, 8, and 9. A typical record of the optical signals specifying the effect of fluid

rheology is given in Fig. 2. As shown in Fig. 8, apparently the initial droplet size does not influence the process of absorption, even if the liquid column is longer than 10 diameters of the capillary. These observations are quite puzzling, because at least for water absorption, an almost developed Poiseuillean profile is expected to be built up in such long columns [19]. Therewith, the droplet volume should affect the flow rate which is in apparent contradiction to the observations. The experimental data show that the viscous forces are somehow counterbalanced, thus maintaining the average velocity unchanged. A quite accurate estimate of the average velocity is given by the Bosanquet value [20]. The Bosanquet velocity U_B can be obtained by writing the momentum balance for the moving column neglecting viscosity and external hydrodynamics [7]. Assuming that the velocity at the inlet is zero and the pressure p^- equals atmospheric pressure, one finds $p^- = p^+ + \rho U_B^2$, where ρ is fluid density. The pressures are connected by the Laplace formula as $p^- - p^+ = 2\sigma\cos\theta/R$, where θ is the contact angle, and σ is the surface tension. Thus, the Bosanquet velocity takes the form $U_B = \sqrt{2\sigma\cos\theta/\rho R}$. In other words, the Bosanquet velocity reflects the balance of the inertial and capillary forces.

The apparent negligibility of viscous forces can be explained if we account for the finite volume of the external droplet [1]. Indeed, the positive Laplace pressure induced by the droplet curvature increases in the process of absorption and may counterbalance the viscous resistance of low-viscosity liquids such as water [21]. A quantitative verification of this idea is presented below.

As seen from Figs. 8 and 9, the velocity reduction is pronounced even for the smallest concentrations of polymer: 10 ppm of PAM gives rise to an almost twofold reduction of the absorption rate. The shear viscosity and the surface tension of the solution of 10 ppm PAM do not differ appreciably as compared with pure water. Thus, the reduction of the absorption rate should be related to the elastic properties of the polymer solution. As we see from the rheological measurements (Fig. 6) in the range of large shear rates the shear viscosity η may be approximated by a constant, which complies with the assumptions of the Maxwell model. We employ the latter to account for fluid elasticity. This model allows us to focus on the effect of polymer additives as that is manifested through the difference in normal stresses at the meniscus. Namely, in addition to the pressure, polymer solutions exhibit an extra stress with a normal component counterdirected to the flow. This effect, known as the Weissenberg effect [22], is inherent in viscoelastic fluids: polymeric coils stretched in a shearing flow oppose the motion.

In the case of relatively long columns, for which the Poiseuillian velocity profile is expected to serve as an appropriate approximation, the physical scenario of the phenomenon is as follows. While moving through a capillary, the column of viscoelastic fluid experiences Poiseuillian resistance similarly to a simple viscous fluid. In addition, in the direction of flow, a normal stress is built up. It is proportional to the pressure gradient squared [16,22,23]. It results in a reduction of capillary pressure at the meniscus, thus lowering effectively the tensile wetting force. As will be shown in a forthcoming paper (Kornev and Neimark [24]), the entrance effect of stretching of a viscoelastic fluid is much smaller than the Weissenberg effect and can be neglected. Mathematically, the kinetics of absorption of a viscoelastic fluid by a capillary is described by the following equation for the position of propagating meniscus x [24]

$$\rho\frac{d}{dt}\left((x+cR)\frac{dx}{dt}\right)+\left(\frac{8\eta}{R^2}\right)x\frac{dx}{dt}+\left(\frac{16\lambda\eta}{R^2}\right)\left(\frac{dx}{dt}\right)^2 = \frac{2\sigma\cos\theta}{R}+\frac{2\sigma}{R_d}+\rho g x. \tag{1}$$

Here c is a coefficient of apparent mass, we assume it to be $c = 1$ [4,25,26]. The first term in the LHS of Eq. (1) accounts for the inertia of the liquid column, the second term is responsible for Poiseuillian friction, the third is caused by the difference in normal stresses at the meniscus of a viscoelastic Maxwellian fluid. The RHS accounts for capillarity and gravity. The first term on the RHS is the capillary pressure at the advancing meniscus and the second term is the Laplace pressure due to the droplet curvature [21]. The radius of the droplet curvature, R_d, is expressed through the current column length x and the droplet volume by using the formulas in Ref. [21]. A detailed discussion of Eq. (1) is given elsewhere [24].

In the beginning of this section, we explained the physical meaning of the Bosanquet velocity by considering the momentum balance. Note that Eq. (1) in the limit of $c = 0$, $\eta = 0$, $\lambda = 0$, and $R_d = \infty$ reduces to the standard equation of capillary fall/rise of an inviscid fluid known as the Bosanquet equation [20]. As shown in [4], the Bosanquet velocity $dx/dt|_{t=0} = U_B = \sqrt{2\sigma\cos\theta/\rho R}$ corresponds to a singular solution to the Bosanquet equation. This solution assumes that the column takes on the characteristic velocity U_B immediately after contact between the fluid and capillary. Accounting for viscosity does not change this singular solution, because the Poiseuillian viscous force is proportional to the length of the liquid column and thus vanishes at $x \to 0$. In the viscoelastic case, the Weissenberg effect contributes to the force balance with a term proportional to the velocity squared. That is in the limit $x \to 0$, $d^2x/dt^2 \to 0$, Eq. (1) with $c = 0$ and $R_d = \infty$ is rewritten as

$$\left(1+\frac{16\lambda\eta}{\rho R^2}\right)\left(\frac{dx}{dt}\right)^2 = \frac{2\sigma\cos\theta}{\rho R}. \tag{2}$$

The solution to Eq. (2) is given by formula

$$U_{\mathrm{VE}} = \sqrt{\frac{2\sigma\cos\theta}{\rho R(1+16\lambda\eta/\rho R^2)}} = \frac{U_B}{\sqrt{1+16\lambda\eta/\rho R^2}}, \tag{3}$$

which determines the velocity of penetration of a viscoelastic fluid in the asymptotic limit when the velocity is still high, but the acceleration ceases. As was mentioned above,

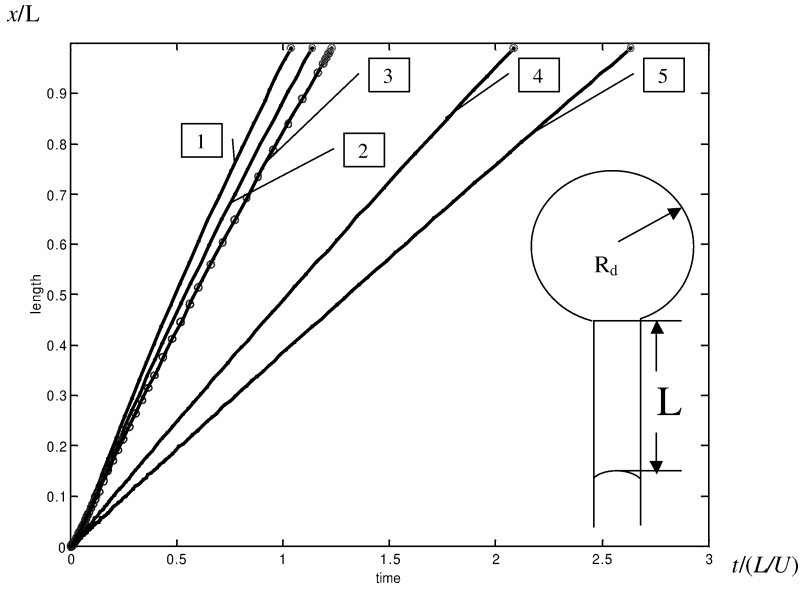

Fig. 10. Kinetics curves of droplet absorption by a glass capillary. Dimensionless coordinate of meniscus, x/L, versus the reduced time, $t/(L/U)$. $c = 1$, $\theta = 0$, $V_0 - V_t = 4$ mm^3, $2R = 0.65$ mm. (1) Water, (2) 10 ppm solution of PEO, (3) 10 ppm solution of PAM, (circles) 10 ppm solution of PAM with a viscosity as in (1) and (2), (4) 100 ppm solution of PAM, (5) 200 ppm solution of PAM.

the Weissenberg effect results in a reduction of the capillary pressure at the meniscus. Therewith, the velocity U_{VE} decreases compared with the Bosanquet velocity U_B. Estimates of the absorption rate based on U_{VE} are presented in Table 1 ($\theta = 0$, $2R = 0.65$ mm) in comparison with the experimental flow rates averaged over the data points of Fig. 8. As seen from Table 1, the velocity of penetration can be estimated by Eq. (3) quite well. This points toward a conclusion that the Weissenberg effect is the primary cause of the reduction in absorption rate.

We studied numerically the role that the fluid viscosity and capillary pressure of the external droplet played in absorption experiments. Leaving the regularizing term with $c = 1$ allows one to formulate "natural" initial conditions for Eq. (1): $x = 0$, $dx/dt = 0$ as $t = 0$. As first shown for viscous fluids in Ref. [25], the model with "natural" initial conditions has the Bosanquet velocity as its limiting case. Thus, the strategy for interpretation of the experimental data is straightforward: we solve Eq. (1) with "natural" initial conditions assuming that the volume of the absorbing droplet at $t = 0$ equals $V_0 - V_t$, and calculate the length of penetration x up to the point when it approaches the maximum length of the liquid column $L = (V_0 - V_t)/\pi R^2$ within a negligibly small distance $\delta = 1 - x/L = 0.001$ to avoid a natural singularity of Eq. (1). The dynamics of meniscus propagation is shown in Fig. 10 for water and PAM solutions of different concentrations for 4-mm^3 droplets. Within time scales relevant to the experiments, the kinetics is almost linear: the Poiseuillian viscous friction is balanced by acceleration due to the Laplace pressure in the external droplet. The velocity depends on the relaxation time due to the Weissenberg effect. To illuminate the effect of the fluid elasticity, we added in Fig. 10 the kinetic curve calculated

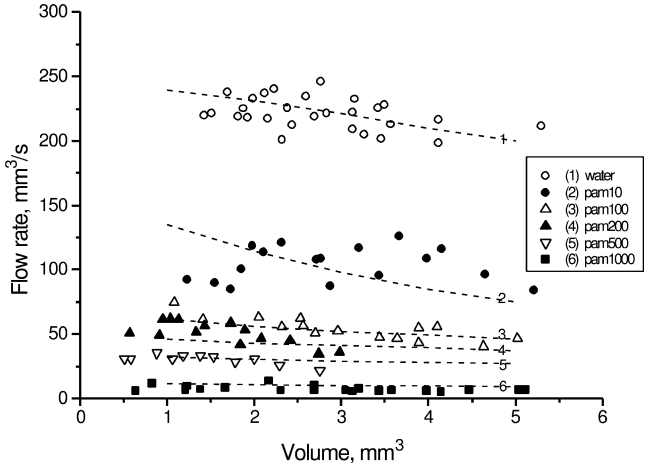

Fig. 11. Comparison of the calculated and experimental rates of absorption. The kinetic curves were calculated with Eq. (1) with the input parameters listed in Table 1.

for a 10 ppm solution of PEO, which has the shear viscosity of water, but the relaxation time is half the relaxation time of a 10 ppm solution of PAM. The circles correspond to a 10 ppm solution of PAM calculated with a shearing viscosity equal to the water viscosity $\eta = 1$ mPa s, which is four times smaller than the experimental value from Table 1. As seen, the viscosity plays a secondary role in the reduction of the absorption rate.

The calculated absorption rates for the droplets of different sizes show a moderate dependence of the rate of absorption on droplet size within the volume range 1 to 5 mm^3. A comparison of theoretical predictions with the experimental data on water and PAM solutions is given in Fig. 11 (dashed lines). As seen, the theory based on Eq. (3) works fairly well. The effects of Poiseuillian friction, gravity, and

capillary pressure of external droplet are responsible for deviations of the curves from their average values. These effects seem to be secondary compared with the effects of inertia and elasticity which determine the initial velocity of penetration, Eq. (3). Note that the calculations were performed without any adjustable parameters!

The predictability of the experimental data for PEO solutions is somewhat poorer than for PAM solutions (see estimates of the rate of absorption in Table 1), especially at high concentrations. This may be related to a known shortcoming of the upper convected Maxwell model as applied to concentrated polymeric systems in shear and extension flows. A similar problem was encountered in earlier studies by Liang and Mackley [27]. The authors concluded that the rheological characteristics determined with the extensional rheotester deviated significantly from those measured with the shear flow cone/plate rheometer. Theoretically, the relaxation time measured with the extensional rheotester is an average over the spectrum of relaxation times measured with the cone/plate rheometer [16,27]. However, the measured relaxation time of extensional deformations systematically exceeded the average relaxation time of shearing deformations, threefold and more. Similarly to the observations of Liang and Mackley [27] to fit the experimental data for 1000 ppm PEO solutions, we would need to use the relaxation time $\lambda = 0.0125$, which is four times smaller than the value in Table 1 measured with the extensional rheotester. This problem requires further investigation.

5. Conclusion

A new technique has been developed to study the kinetics of absorption of fluids by porous substrates. Using an optical electronic measuring system with millisecond resolution, we monitored the process of absorption of a single droplet of a given volume. The time of droplet absorption characterizes the material absorbency. The method capabilities are demonstrated in examples of absorption of water and polymer solutions by glass capillaries. Aqueous solutions of polyethyleneoxide (PEO) and polyacrylamide (PAM) were chosen as model viscoelastic fluids.

As shown in experiments on capillaries, the presence of a small amount of polymer additives causes a significant increase in the time of absorption. We conclude that the fluid elasticity is responsible for the prominent reductions in the rate of absorption of polymer solutions. We introduced a modified Bosanquet formula, Eq. (3), for the velocity of penetration and showed that the average velocity of absorption of droplets with different volumes is well described by this formula. The introduced formula represents a balance between the wetting, inertial, and elastic forces in the asymptotic regime $x \to 0$, when the velocity is high, but the acceleration of the liquid column diminishes. It assumes that a counterpressure due to fluid elasticity weakens the driving capillary pressure at the meniscus.

To describe the kinetics of droplet penetration in more detail we used a generalized Lucas–Washburn equation, Eq. (1). This equation, derived and discussed in detail elsewhere [24], allows us to take into account the effects of the viscous friction due to the Poiseuillian flow inside the capillary and of the acceleration of the flow caused by the Laplace pressure induced by the positive curvature of the external droplet. These effects are shown to be secondary compared with the wetting, inertial, and elastic forces. Remarkable agreement was found for the rates of absorption of water and PAM solutions, including droplet volume dependence. With the physical parameters of fluids measured independently, the data are fitted without any adjustable parameters. For PEO solutions, we observed the same trend as for PAM solutions; however agreement between theoretical predictions and the experiments was poorer, especially for high concentrations. Possible reasons for these deviations are discussed.

Also, we report visualization experiments on absorption of water and polymer solutions by sugar cubes as an example of porous substrates. Although the kinetics of droplet adsorption by porous substrates is similar to the kinetics of droplet adsorption by capillaries, an interpretation of experimental data is more complex and requires a plausible hydrodynamic model for the lateral spreading in pores.

Acknowledgments

The work is sponsored by the Johnson & Johnson Focused Giving Program. A.V.B. and A.N.R. acknowledge RFBR for partial support via Grants 99-01-00957 and 99-01-00474.

References

[1] A. Marmur, Adv. Colloid Interface Sci. 39 (1992) 13.
[2] S. Middleman, Modeling Axisymmetric Flows: Dynamics of Films, Jets, and Drops, Academic Press, New York, 1995.
[3] E. Kissa, Textile Res. J. 66 (1996) 660.
[4] K.G. Kornev, A.V. Neimark, J. Colloid Interface Sci. 235 (2001) 101.
[5] X. Chen, K.G. Kornev, Y.K. Kamath, A.V. Neimark, Textile Res. J. (2001) 71.
[6] A.A. Jeje, J. Colloid Interface Sci. 69 (1979) 420.
[7] D. Quere, Europhys. Lett. 39 (1997) 533.
[8] A. Hamraoui, K. Thuresson, T. Nylander, V. Yaminsky, J. Colloid Interface Sci. 226 (2000) 199.
[9] R.K. Holman, M.J. Cima, S.A. Uhland, E. Sachs, J. Colloid Interface Sci. 249 (2002) 432.
[10] MRS Bull. 26 (2001).
[11] A.W. Adamson, A.P. Gast, Physical Chemistry of Surfaces, 6th ed., Wiley, New York, 1997.
[12] Y. Amarouchene, D. Bonn, J. Meunier, H. Kellay, Phys. Rev. Lett. 86 (2001) 3558.
[13] R.B. Bird, R.C. Armstrong, O. Hassanger, Dynamics of Polymeric Liquids. Fluid Mechanics, Vol. 1, Wiley, New York, 1987.
[14] A.V. Bazilevsky, V.M. Entov, A.N. Rozhkov, Polym. Sci. A 43 (2001) 716.

[15] A.V. Bazilevsky, V.M. Entov, A.N. Rozhkov, Liquid filament microrheometer and some of its applications, in: The Golden Jubilee Meeting of the British Society of Rheology and Third European Rheology Conference, Edinburgh, UK, 1990.
[16] S. Middleman, Fundamentals of Polymer Processing, McGraw–Hill, New York, 1977.
[17] A.V. Bazilevsky, V.M. Entov, M.M. Lerner, A.N. Rozhkov, Polym. Sci. A 39 (1997) 316.
[18] G.H. McKinley, A. Tripathi, J. Rheol. 44 (2000) 653.
[19] H. Schlichting, Boundary-Layer Theory, 6th ed., McGraw–Hill, New York, 1968.
[20] C.H. Bosanquet, Philos. Mag. 45 (6) (1923) 525.
[21] A. Marmur, J. Colloid Interface Sci. 722 (1988) 209.
[22] K. Weissenberg, Nature 159 (1947) 310.
[23] V.A. Gorodtsov, V.M. Yentov, J. Appl. Math. Mech. 61 (1997) 111.
[24] K.G. Kornev, A.V. Neimark, J. Colloid Interface Sci. (2002).
[25] J. Szekely, A.W. Neumann, Y.K. Chuang, J. Colloid Interface Sci. 35 (1971) 273.
[26] E. Lorenceau, D. Quere, J.Y. Ollitrault, C. Clanet, Phys. Fluids 14 (2002) 1985.
[27] R.F. Liang, M.R. Mackley, J. Non-Newton. Fluid Mech. 52 (1994) 387.